Drying Technology
An International Journal

ISSN: 0737-3937 (Print) 1532-2300 (Online) Journal homepage: www.tandfonline.com/journals/ldrt20

Simulation of the water mass transport in electrodes during post-drying and moisture management of Li-ion battery production via the Two-Scale-Model

Thilo Heckmann, Philipp Barbig, Anh Thi Pham, Jochen C. Eser, Philip Scharfer & Wilhelm Schabel

To cite this article: Thilo Heckmann, Philipp Barbig, Anh Thi Pham, Jochen C. Eser, Philip Scharfer & Wilhelm Schabel (23 Feb 2026): Simulation of the water mass transport in electrodes during post-drying and moisture management of Li-ion battery production via the Two-Scale-Model, Drying Technology, DOI: 10.1080/07373937.2026.2631674

To link to this article: https://doi.org/10.1080/07373937.2026.2631674

DRYING TECHNOLOGY
https://doi.org/10.1080/07373937.2026.2631674

Taylor & Francis
Taylor & Francis Group

Simulation of the water mass transport in electrodes during post-drying and moisture management of Li-ion battery production via the Two-Scale-Model

Thilo Heckmann, Philipp Barbig, Anh Thi Pham, Jochen C. Eser, Philip Scharfer, and Wilhelm Schabel

Thin Film Technology (TFT), Karlsruhe Institute of Technology (KIT), Karlsruhe, Germany

ABSTRACT

The moisture content of the material inside a lithium-ion battery (LiB) cell is a critical parameter for safety and performance of LiBs. Post-drying or final drying prior to filling the cell with electrolyte reduces the water content within the cell to an appropriate level, while moisture management aims to control the water content along the production chain. In both cases, the sorption of water in the composite structure of the porous electrode is the physical phenomenon that must be understood to design and adjust process parameters for post-drying and moisture management. It is our hypothesis that this sorption of water in the electrode can be simulated with a phenomenological mass transport model on two scales. Therefore, we introduce the Two-Scale-Model which couples the mass transport on micro scale (e.g., the polymeric binder phase of the electrode) and macro scale (e.g., the gas phase inside the electrode). Experimentally, a magnetic suspension balance refitted to measure vacuum drying curves with a customized sample holder provides validation data. The results of the Two-Scale-Model show that the mass transport on micro and macro scale can be characterized by the diffusion times of micro and macro scale. The Two-Scale-Model is theoretically validated by comparing its boundary cases with one-dimensional mass-transport models and experimentally validated by comparing the simulation results to experimental data. It is successfully applied to desorption of water from a LiB anode, which shows that the differentiation between micro- and macro-scale sorption is a feasible approach to describe the water mass transport in a LiB anode.

ARTICLE HISTORY
Received 30 September 2025
Revised 7 February 2026
Accepted 10 February 2026

KEYWORDS
Post-drying; Li-ion batteries; sorption; moisture management

Introduction

Lithium-ion batteries (LiBs) are prone to degradation by water and other species of the production atmosphere, which are carried into the cell *via* sorption processes during production and as residual solvent in case of water-based processing.[1–3] Moisture management and post-drying are measures to control the water uptake and mitigate this degradation during the production of LiB. The mitigation strategy of these measures is situating the production of LiB-electrodes in demand-oriented conditioned environments.[1,4–6] Providing these environments during mass production is energy demanding and cost intensive, and therefore increases the ecological footprint of the life cycle of LIB.[7–9] Designing the moisture management and post-drying demand-oriented requires a precise understanding of the occurring physical phenomena[2,6,10–13] and is essential to reduce cost and ecological footprint of the life cycle of LiB.

Several sorption mechanisms and associated kinetics occur during the interaction of an electrode and its components with the atmosphere of the production environment.[6,12,14–18] Both physical and chemical sorption occur in the components of LiB.[10,19,20] Understanding these mechanisms is necessary to predict the interaction of LiB components and atmosphere. The mass transports that may kinetically limit the sorption of LiB components are crucial to assess severity of exposure to critical atmospheres and designing a demand-oriented moisture management and post-drying.[6]

The sorption and its mass transport of water inside an electrode during production have been addressed by many studies. Eser et al. showed that specifically the anode binder carboxymethyl cellulose (CMC) absorbs large quantities of water compared to other components of this electrode.[10,11] In an additional study, they examined the mass transport of water

CONTACT Thilo Heckmann thilo.heckmann@kit.edu Thin Film Technology (TFT), Karlsruhe Institute of Technology (KIT), Karlsruhe 76131, Germany
Supplemental data for this article can be accessed online at https://doi.org/10.1080/07373937.2026.2631674.

inside this polymeric binder *via* experiments and simulation.[12] Huttner et al.[6] proposed a post-drying routine based on approximations of the desorption processes about the drying time of a vacuum drying in coil format. Kosfeld et al.[16] investigated the kinetics of water in electrodes and separator from an industrial perspective, proposing a post-drying strategy individual for anode, cathode, and separator. Stich et al.[21] measured water uptake kinetics of electrodes, providing an overview for various electrodes. Heckmann et al. compared different binder systems regarding their effect on vacuum coil post-drying and evaluated gas phase resistances during this process.[14,22] The aforementioned studies either provide insight into individual kinetics of electrode post drying or describe the mass transport during post drying as one mass transport. The scope of this study to propose a mass-transport model that accounts for the individual mass transports inside the composite structure of a LiB in one model.

It appears plausible that the mass transport of, for example, water in an anode during the post drying in coil format is affected by multiple individual mass transport resistances on different lengths scales. The lengths scales could be the mass transport of water in the polymeric binder CMC as a micro scale. Compared to this micro scale the mass transport of water through the gas phase of the porous structure of the anode could be the mass transport on macro scale. The polymeric binder, for example, was estimated to have an average thickness ranging from 0.1 to 1 µm.[12] In contrast, the mass transport through the porous structure of an electrode spans in the centimeter range, in certain process steps.[6,16] We hypothesis that the different length scales of the mass-transport resistance in every component require at least a two-scale simulation to account for the geometry of an electrode. These two scales are a micro and a macro scale. This study aims to consolidate available research into a suitable mass-transport model of water inside an electrode that incorporates the individual mass-transport resistances in various geometries. This mass-transport model covers post-drying and exposure of free-standing electrodes as well as electrodes in coils and stacks. Post-drying experiments from a magnetic suspension balance with a model anode serve as validation for the simulation. The model is universally derived for an electrode structure with various sorptives; however, experiments and simulation are carried out for one model anode with a polyvinylidene fluoride (PVDF) binder system and water.

Materials and methods

Materials

Anodes of LIB served as sample for the post-drying experiments. PVDF anodes were prepared according to Jaiser et al.[23]

Simulation

The partial differential equation (PDE) solver "D03PPF" from the Numerical Algorithms Group Library (NAG, Oxford, United Kingdom) solves the PDEs on micro and macro scale. The PDEs on micro scale are manually discretized over the space coordinate x and solved as a system of ordinary differential equation. The numerical solution of the PDEs on micro scale is conducted by the method of lines.[24]

Experimental setup

A sorption apparatus with a magnetic suspension balance (TA waters GmbH, Germany) measures the experimental data. This apparatus can operate with the pure vapor method after Schabel[10–12,25] and a vacuum drying mode.[14,22] The experiments of this study were performed with a modification for the vacuum drying mode according to Figure 1(a): Glass spheres (diameter 4 mm, Carl Roth GmbH & Co. KG, Germany) increase the pressure drop at the bottom of the measurement cell. Furthermore, the glass spheres spread the gas flow into the measurement cell from the cross section of the inlet pipe to the cross section of the measurement cell. Therefore, the glass spheres homogenize the flow field inside the measurement cell and stabilize the mass signal of the scale.

Experimental procedure

One vacuum-drying experiment consists of several consecutive steps. At first the sample is dried at 90 °C in dry nitrogen (dew-point temperature: > -60 °C) to determine the dry mass of the sample. Subsequently, the sorption apparatus is operated with the pure vapor method, which creates an atmosphere with a relative humidity of 55%. The sample absorbs water according to the water activity of this atmosphere. Once the sample reached its sorption equilibrium with the surrounding atmosphere, the vacuum drying mode can be initiated by engaging the vacuum pump and nitrogen flow. The mass of the sample is monitored during this entire procedure. Therefore, the dry mass of the sample, the initial loading before vacuum drying, and the time-resolved vacuum-drying curves are obtained.

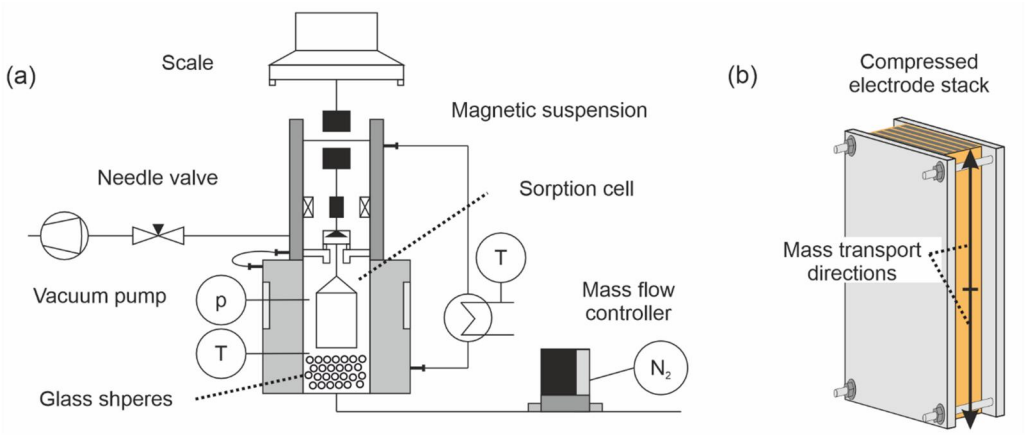

Figure 1. (a) Experimental setup in vacuum drying mode consists of a sorption cell and a magnetic suspension balance. Vacuum pump, needle valve, glass spheres, and mass flow controller facilitate the perfusion at various pressures. (b) Electrode stack as sample for the desorption experiments. Aluminum plates (gray) compress the electrodes. The copper foil (orange) acts as a diffusion barrier, navigating the mass transport according to the arrow. The short side of this stack is open for mass transport.

Sample

The sample configuration was developed for this study to mimic the mass transport inside a coil or electrode stack while being light enough to operate below the weighing limit of the magnetic suspension balance. A stack of anodes made with a PVDF binder system serves as sample for the post-drying experiments. The sheets of the electrodes were cut, folded, and aligned to form a stack. This stack is closed on the long side and has a phase boundary (porous electrode – gas phase) on the short side (compare Figure 1(b)). This configuration maximizes the mass-transport distance through the porous structure for molecules either sorbing or desorbing from the sample. The stack of anodes was placed and pressed between two aluminum plates. The thickness of the electrode stack must be equal to the combined thickness of all the stacked electrodes. The aluminum plates were perforated to reduce weight while maintaining structural integrity (not shown in Figure 1(b)). This configuration assures that molecules must be transported through the porous electrodes.

Simulation model

Figure 2(a) shows the electrode stack that is used as a sample in this study and the boundary conditions that are applied during the simulation of the vacuum drying of this electrode stack. A cross section of an electrode sheet that is enclosed in the electrode stack is shown in Figure 2(b), which outlines the two-dimensional structure of an electrode. The gas phase in the porous structure is the mass-transport resistance on macro scale (mass-transport distances ~ cm for post-drying in coil format).[6,16] Along this macro scale, many sorption phenomena on micro scale occur, e.g. in the binder phase (mass-transport distance ~ µm).[12] Sorption phenomena on micro scales act as source terms for the mass transport on macro scale, distributed in mass-transport direction on macro scale. This configuration is comparable to sorption in a porous structure with inter- and intra-particle mass-transport resistances.[26] The proposed simulation model incorporates the influence of sorption on micro and macro scale on the overall mass transport of water in an electrode. This simulation is applicable to roll-to-roll, coil, and stack post-drying as well as to the simulation of water sorption during production. The processes described by the simulations in this study are considered isothermal. The electrode considered in this paper is the anode.

The Two-Scale-Model couples transient mass transport on micro and macro scale that are represented by one-dimensional PDEs. The mass transport on macro scale, discretized along the z-axis, has its mass-transport direction along the long side if the electrode stack (compare Figure 2(c)). Between every two mesh points on macro scale, a PDE, representing mass transport on micro scale, couples as a source term into the mass transport on macro scale.

A mass balance of water in the electrode provides the basis for the mass-transport calculation on micro and macro scales. The balance domain is subdivided into micro and macro scale as well as solid and gas phase on the macro scale. The solid phase on macro scale refers to the graphite and carbon black particles. The only relevant mass transport in z-direction is

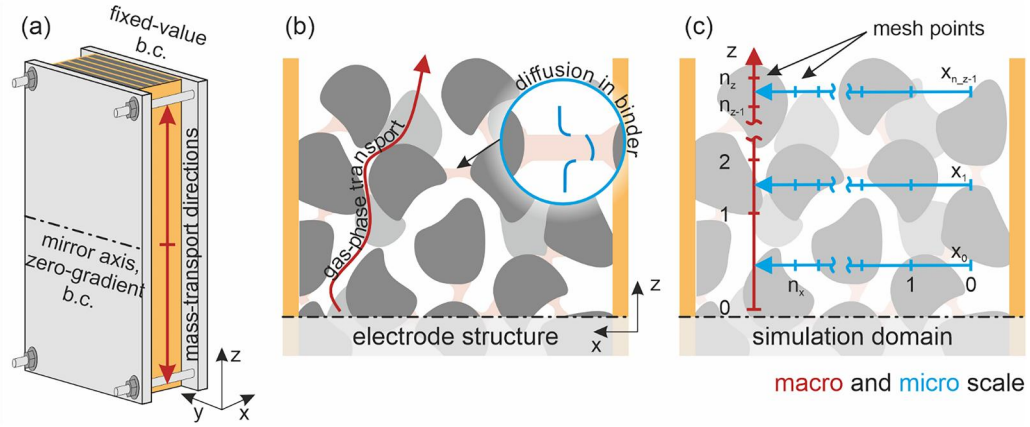

Figure 2. (a) shows the electrode with applied boundary conditions (b,c) at the mirror axis (dash-dot line) and the phase boundary. (b) shows the cross section of one electrode sheet from within the electrode stack enclosed in between orange copper foil (sample preparation compare Figure 1). Possible mass-transport phenomena on macro and micro scale are depicted in the electrode structure schematically. The mass transport can be abstracted by a two-scale simulation mesh, shown in (c). The simulation mesh on the macro scale is represented by the interrupted arrow in red. Mesh points range from 1 to n_z and are unevenly distributed to stabilize the simulation close to the phase boundary, where concentration gradients are steep. The simulation mesh on the micro scale is represented by the interrupted arrows in blue. Mesh points on micro scale are also unevenly distributed and range from 1 to n_x. This simulation mesh is the basis for the Two-Scale-Model discussed in this study.

assumed to be gas-phase mass transport through the porous structure of the electrode.[10,14]

$$\underbrace{\Phi\left(\varepsilon\frac{\partial C_{i,Ma,g}}{\partial t}+(1-\varepsilon)\frac{\partial C_{i,Ma,s}}{\partial t}\right)}_{\text{macro scale}}+\underbrace{(1-\Phi)\frac{\partial C_{i,Mi}}{\partial t}}_{\text{micro scale}}=\underbrace{\Phi\ \varepsilon\frac{\partial}{\partial z}D_{i,Ma}\frac{\partial C_{i,Ma,g}}{\partial z}}_{\text{macro scale}} \tag{1}$$

The indices are: i – sorptive, g – gas phase, s – solid phase, Ma – macro scale, and Mi – micro scale. The variables t and z represent time and space coordinates on macro scale. The concentration is c. $D_{i,Ma}$ is the diffusion coefficient of the solvent i, water in the gas-phase in the porous structure (macro scale). The time derivative, or accumulation term, is divided according to the phases inside the electrode (compare Kärger[26]). The quantities Φ and ε denote the volume fractions that distribute the phases in the simulation domain. The porosity ε distinguished gas and solid phase on macro scale. Φ indicates the volume distribution of the micro and macro scale (similar concept as the porosity). The mass transport on micro scale of the anode is a source term in the PDE on macro scale. If $\Phi = 1$, there is no mass-transport resistance on micro scale. The mass transport on macro scale predominately occurs in the gas phase (omitting possible surface diffusion on the solid phases) and in the polymeric binder. Equation (2) shows the PDE:

$$\begin{aligned}&\Phi\left(\varepsilon\ K_{Sorption,Ma}\frac{\partial c_{i,Ma,s}}{\partial t}+(1-\varepsilon)\frac{\partial c_{i,Ma,s}}{\partial t}\right)\\&+(1-\Phi)\frac{\partial c_{i,Mi}(z)}{\partial t}\\&=\Phi\ \varepsilon\ K_{Sorption,Ma}\frac{\partial}{\partial z}D_{i,Ma}\ \frac{\partial c_{i,Ma,s}}{\partial z}\end{aligned} \tag{2}$$

For the simulation of the drying experiment with the electrode stack, $D_{i,Ma}$ is approximated with a model that includes molecular diffusion and Knudsen diffusion based on the Knudsen number of the gas phase in the porous structure on macro scale. This model for the diffusion coefficient was validated on a similar structure (for details see[14]) and adapted to the electrode structure *via* its porosity and mean pore diameter along with process parameters pressure and temperature. The porosity is calculated from the solid density of electrode and the weight of an electrode of know size and weight. The mean pore diameter of the porous structure was approximated by 2.5 µm based on experimental data from mercury intrusion pore size analysis. A linear sorption equilibrium describes the sorption of water on the solids at the gas–solid interface on macro scale. The sorption constant $K_{Sorption,Ma}$ correlates the water content of the solid phase to the water content of the gas phase. This is a simplification because the sorption equilibria of water in battery material are complex.[11] This simplification is necessary to have constant diffusion times and proportionality constants, which allows comparing the results of micro and macro scale mass transport.

Nevertheless, the non-linear sorption equilibria can be incorporated into the PDEs as the PDEs are numerically solved.[14] $K_{Sorption,Mi}$ (shown in Equation 5) is the sorption constant that correlates the water content on macro scale to the water content on micro scale.

In summary, the following physical quantities required for the Two-Scale-Model are experimentally determined for the comparison of the simulation results to the experiments: Sorption constants, porosity on macro scale, mean pore diameter macro scale, mass transport distance on macro scale. Based on these quantities, the tortuosity and diffusion coefficient on macro scale are modeled. The value of mass-transport parameters on micro scale are fitted to the drying experiment, which is discussed in the results section.

The linear sorption equilibrium is assumed to adjust immediately at every mesh point. The term containing the time derivative of the sorptive loading on micro scale is the source term that couples micro-scale and macro-scale equations. The PDE of the diffusion of sorptive on micro scale is given in Equation (3) as follows:

$$\frac{\partial c_{i,k,Mi}(z)}{\partial t} = \frac{\partial}{\partial x_k}\left(D_{i.Mi}\ \frac{\partial c_{i,k,Mi}}{\partial x_k}\right) \tag{3}$$

The nomenclature follows Equation (1). x_k is the space coordinate on micro scale, indexed by k – the number of PDE on micro scale distributed on macro scale. $D_{i.Mi}$ is the diffusion coefficient of water in the polymeric binder (micro scale). Both PDEs are numerically solved. The zero-gradient boundary condition applies to position 0 on macro scale due to the configuration of the sample holder (compare Figure 2). The simulation domain ranges from the middle of the anode stack to the phase boundary at the short edge of the anode stack in mass-transport direction (compare Figure 2). Therefore, the middle of the anode stack can be considered as a mirror axis. The Dirichlet boundary condition (fixed value) applies to the phase boundary of the anode stack. The simulation domain of the mass transport on micro scale is more abstract and represented by an effective simulation domain on micro scale. The idea is to approach the mass transport of the water in e.g., the complex binder matrix inside an electrode with an effective mass-transport distance. The boundary conditions applied to this domain are the zero-gradient boundary condition on side and the fixed-value boundary condition on the other side of the domain, where micro and macro scale are coupled. The PDE on macro scale is discretized on the z-axis with n_z number of mesh points. Between every two mesh points of the z-axis an individual PDE on micro scale is discretized, which results in a total of $n_z - 1$ PDEs on micro scale and one PDE on macro scale. The number and position of the mesh points are determined by an algorithm that takes the mass-transport distance on each scale into account. The algorithm generates a non-equidistant mesh, with smaller mesh-point distance at the phase boundary where the concentration gradients are steep. The PDEs on micro and macro scale share the same time axis, which couples the PDEs. The number of mesh points and other physical quantities used for the simulations for each of the figures in the results section are listed in the supporting information.

Results and discussion

The Two-Scale-Model, coupling mass transport on macro and micro scale of the composite structure of an electrode, is proposed to describe the transport of e.g. water inside a battery electrode during moisture management and post-drying. Figure 3 shows three configurations of mass-transport resistances on macro and micro scale and their arrangement inside an electrode. The resistances vary in significance, indicated by arrow weight relative to each other. In the following, the mass transport of water in an anode is considered.

Configuration (a) shows the case where the limiting mass-transport resistances inside the electrode is the one on micro scale. This could be the case for an electrode with a CMC/styrene butadiene rubber (SBR) binder system (compare Eser et al.[12]) and for free standing electrodes. Configuration (c) is the opposite of (a) where the restricting mass transport is the one on macro scale. This could be the case in coil-format post-drying. In configuration (b), the mass-transport resistances on both scales are in the same order of magnitude and mutually affect the mass transport of an electrode. In this case, it is hypothesized that mass transport on both scales must be considered in a model which couples the mass transport on micro and macro scale to predict the mass transport of e.g., water in an anode correctly.

The diffusion times on micro and macro scale show which scale determines the mass transport inside the electrode structure. The measure "diffusion time" of mass transport on micro scale (3) and macro scale (4) is proposed with mass-transport parameters as follows:

$$\tau_{\mathrm{micro}} = \frac{s^2_{\mathrm{micro}}}{D_{i,\mathrm{micro}}}. \tag{4}$$

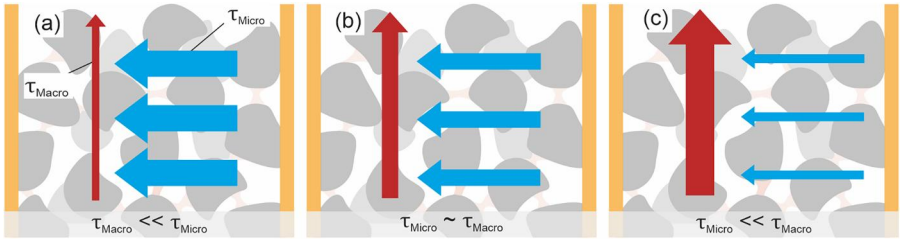

Figure 3. Schematic of mass-transport resistances on macro and micro scale inside the composite structure of a battery electrode. Depending on the water uptake mechanisms on macro and micro scale and the process parameters (pressure, temperature, etc.) either one or both scales affect the mass transport inside the battery electrode. The diffusion times τ_{macro} and τ_{micro} quantify the mass-transport kinetics. Comparing the diffusion times shows whether the mass-transport resistance on either the macro or micro scale is dominant. (a) shows the case where the mass transport on micro scale determines the mass transport of an electrode. (c) is the opposite. (b) shows the case where the mass transport on macro and micro scale affects the mass transport of an electrode.

This equation omits the mass transport on macro scale entirely. $D_{i,\mathrm{Micro}}$ is the diffusion coefficient of component i on the micro scale (in this case the polymeric binder matrix). s_{micro} is the mass-transport distance on micro scale. If the micro scale is the binder matrix of the electrode, s_{mirco} would be the thickness of the binder. This thickness of the binder structure is a distribution and to our knowledge difficult to determine. Based on previous studies, the thickness is in the nanometer to micrometer range.[27] In this case, s_{mirco} could be approximated *via* a representative binder thickness.

The diffusion time on macro scale must include the water that is present on micro scale. Because of the configuration of an electrode, water desorbing on micro scale affects the mass transport on macro scale. The mass transport on only the macro scale can be derived from Equation (2) by neglecting the mass transport on micro scale. This means that the mass transport on micro scale is fast compared to the mass transport on macro scale. Therefore, the water concentration on micro scale is not a function of the space coordinate on micro scale x and can be converted *via* the sorption constant ($K_{\mathrm{Sorption},Mi} \cdot c_{i,Ma,s} = c_{i,Mi}$). The water on micro scale is included in the accumulation term of Equation (5) with the respective sorption constant. The diffusion time τ_{macro} is then given in Equation (6).

$$\left[\Phi \cdot \left(\varepsilon \cdot K_{\mathrm{Sorption},Ma} + (1-\varepsilon)\right) + (1-\Phi) \cdot K_{\mathrm{Sorption},Mi}\right] \cdot \left(\frac{\partial c_{i,Ma,s}}{\partial t}\right) = \Phi \cdot \varepsilon \cdot K_{\mathrm{Sorption},Ma} \cdot D_{i,Ma} \cdot \frac{\partial^2 c_{i,Ma,s}}{\partial z^2} \quad (5)$$

Apart from the transport parameters (diffusion coefficient and transport distance), volume fractions and sorption coefficients must be included. s_{marco} is the distance a water molecule must travel to exit the electrode. For the experiment of this study, halve the distance of the electrode stack, compare Figure 1(b) (centimeter range). Φ is the volume distribution between the macro and micro scale, ε is the porosity on macro scale. Linear sorption equilibria describe the sorption equilibria at the phase boundaries using the sorption constants $K_{\mathrm{Sorption},Ma}$ (solid–gas interface on macro scale) and $K_{\mathrm{Sorption},Mi}$ (interface micro and macro scale).

Boundary case: macro scale controlled

For a defined mass-transport resistance on macro scale, the fastest desorption of water from the electrode is possible, if the mass transport on micro scale is neglectable. The following theoretical consideration compares solutions of the Two-Scale-Model with various diffusion times to the solution of the PDEs with the mass-transport resistance purely on the macro scale. The diffusion time on macro scale is constant and the same as in the simulation of pure macro scale. The diffusion time on micro scale is either the same as the diffusion time on macro scale or deviates by a factor of 10 and 0.1. The solution of the PDE on macro scale (Equation 2) without any mass-transport resistance on micro scale marks the fasted desorption (no τ_{Mirco}). This solution of the PDEs with the mass-transport resistance purely on the macro scale is equivalent to the simulation of the one-dimensional

$$\tau_{\mathrm{macro}} = \frac{\left[\Phi \cdot \left(\varepsilon \cdot K_{\mathrm{Sorption},Ma} + (1-\varepsilon)\right) + (1-\Phi) \cdot K_{\mathrm{Sorption},Mi}\right] \cdot s_{\mathrm{Macro}}^2}{\Phi \cdot \varepsilon \cdot K_{\mathrm{Sorption},Ma} \cdot D_{i,\mathrm{macro}}}. \quad (6)$$

diffusion equation. Figure 4 shows these results for a volume distribution between micro and macro scale of 50:50. The mass transport parameters for this simulation are given in the SI. The water is equally distributed on both scales.

Figure 4 plots the overall concentration of water in the electrode over time. The desorption starts at $C_{w,0}$ and equilibrates at $C_{w,\infty}$. The solution of the boundary case "pure macro scale" and the solutions of the Two-Scale-Model are plotted in red and black, respectively. The diffusion times for each solution are directly linked to the individual graphs. $\tau_{macro} \gg \tau_{micro}$: If the diffusion time on micro scale is 10-times smaller than the diffusion time on macro scale, the simulation of the Two-Scale-Model approaches the solution of Equation (2) without a mass-transport resistance on micro scale (no τ_{micro}). For this and larger ratios of the diffusion times, the mass transport of water inside the anode can be approximated with the PDE of pure macro scale.

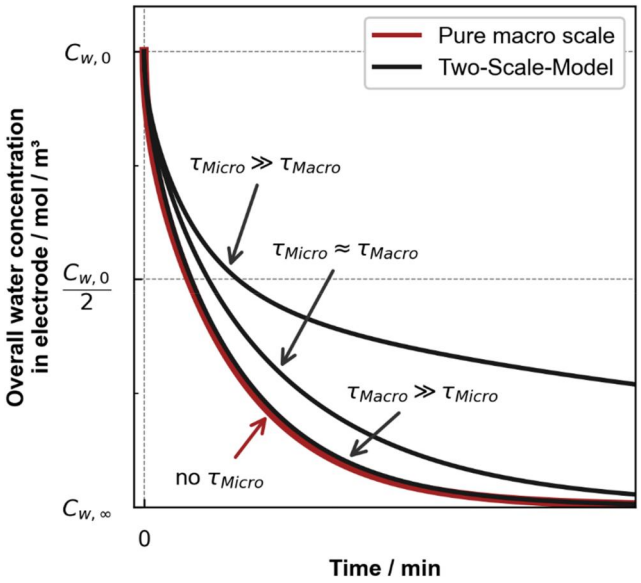

Figure 4. Solutions of the Two-Scale-Model for a desorption from $C_{w,0}$ to $C_{w,\infty}$ (exact values, see SI). τ_{micro} varies. The boundary case of a pure macro scale desorption shows the desorption according to Equation (2) without a mass-transport resistance on micro scale (no τ_{micro}). The solutions of the Two-Scale-Model show results with τ_{micro} that is either larger by factor 10 compared to, smaller by factor 0.1 compared to, or equal to τ_{macro}. With decreasing τ_{micro}, the Two-Scale-Model approaches the pure macro-scale solution, which shows that the Two-Scale-Model replicates this boundary correctly. The solution of the Two-Scale-Model with increased τ_{micro} does not reach $C_{w,\infty}$ within the plotted time frame.

The solution of the Two-Scale-Model for $\tau_{macro} \approx \tau_{micro}$ exhibits a curve-shape that deviates from the boundary case with no τ_{micro}. A pure macro scale simulation with a single constant diffusion coefficient cannot reproduce the solution of the Two-Scale-Model for $\tau_{macro} \approx \tau_{micro}$ (this matter will be further addressed below). This shows that the Two-Scale-Model is necessary to replicate the desorption correctly if macro and micro scale both influence the mass transport of water in the anode. The solution of the Two-Scale-Model for the desorption with $\tau_{micro} \gg \tau_{macro}$ does not equilibrate in the plotted time frame. This desorption curve transitions into a nearly linear degression after surpassing $\frac{C_{w,0}}{2}$, which is the concentration of water on micro scale.

The desorption of the first halve of the water concentration in the electrode (above $\frac{C_{w,0}}{2}$) is less affected by the variation of the diffusion time on micro scale than the second halve of the water concentration in the electrode (below $\frac{C_{w,0}}{2}$). This shows, as expected from Equation (2), that the mass transport of water

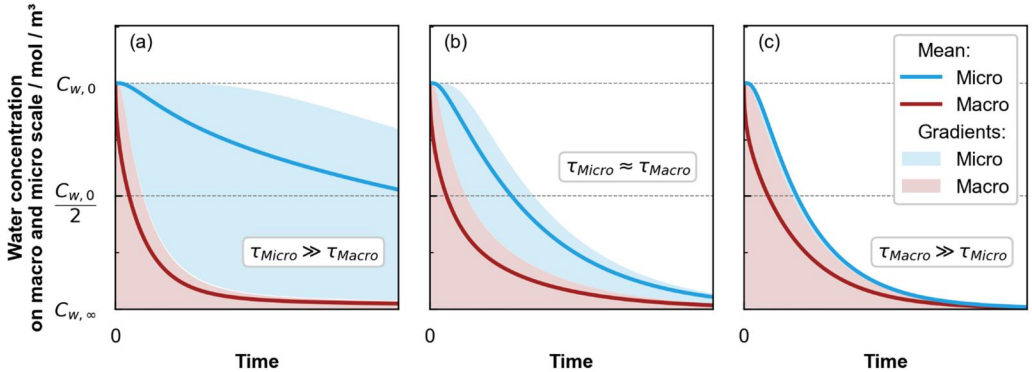

Figure 5. Solutions of the Two-Scale-Model for a desorption from $C_{w,0}$ to $C_{w,\infty}$ from Figure 4. The gradients of the water concentration on macro and micro scale are indicated by the colored areas. The extent of these gradients shows whether the mass transport on macro scale or the mass transport on micro scale dominates the mass transport of water in the electrode. (a) shows the concentration gradients of solution $\tau_{micro} \gg \tau_{macro}$ with large concentration gradients on micro-scale and compared to the concentration gradients on macro scale. Concentration gradients on both scales develop for $\tau_{micro} \approx \tau_{macro}$ (b). The only visible concentration gradients in (c) are the ones on macro scale.

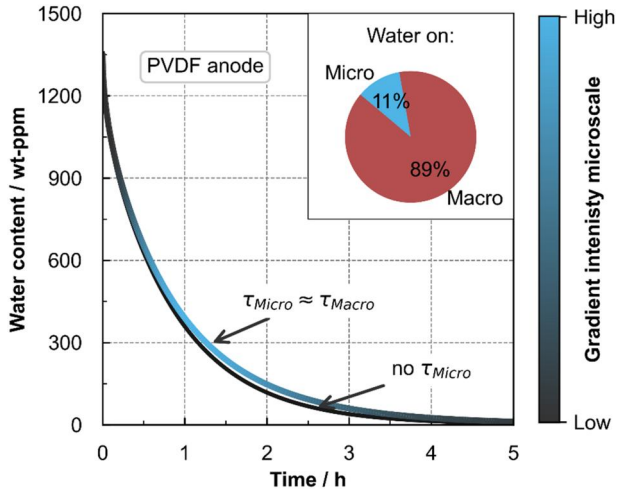

Figure 6. Solution of the Two-Scale-Model for a desorption of the PDVF anode with $\tau_{micro} \approx \tau_{macro}$ and the solution of pure macro scale (no τ_{micro}). The water is distributed among the macro and micro scale according to the pie chart. Electrode composition and water distribution are adapted from literature. The color bar indicates the normalized concentration gradient intensity on micro scale. Blue indicates that the concentration gradients are developed. Both desorption curves propagate alike. The solution of the Two-Scale-Model deviates from the pure macro scale solution after one hour. Overall, the effect of the mass transport on micro scale is small compared to Figure 4.

on macro scale does not strongly depend on the mass-transport resistance on micro scale.

These results show that the shape of the desorption curve yields information about the diffusion times inside the electrode given the arrangement of the scales as shown in Figure 2 is plausible. If the desorption data resembles the desorption data simulated with one mass-transport resistance, the mass transport on either micro or macro scale dominates the mass transport of water in the electrode. If the sorption has a clear deceleration and transitions into a linear, the mass transport on micro and macro scale contributes to the overall mass transport. Numerically, the solutions of the Two-Scale-Model for $\tau_{macro} \approx \tau_{micro}$ and $\tau_{macro} \ll \tau_{micro}$ cannot be reproduced by a one-scale simulation with a constant diffusion coefficient. If the diffusion coefficient changes the simulated desorption is stretched or compressed along the x-axis but does not change shape.

The boundary case for pure micro scale desorption is provided in the SI. The diffusion time on macro scale is either the same as the diffusion time on micro scale or deviates by a factor of 10 and 0.1. The solution obtained from the Two-Scale-Model for these three cases are compared to the solution of the one-dimensional diffusion equation on micro scale. The results are like the results in Figure 4 – the solution of the Two-Scale-Model with $\tau_{macro} \ll \tau_{micro}$ approaches the pure micro scale solution, which shows this boundary case can also be replicated with the Two-Scale-Model.

Gradients of the water concentration during the pure macro scale boundary case

Concentration gradients develop during transient mass transport and describe the difference of the concentration of the transported species between two boundary interfaces. In the solution of the Two-Scale-Model, gradients of the water mass transport in an electrode develop on macro and micro scale. These gradients indicate how strongly mass transport on either the macro or micro scale affects the mass transport of water in the electrode. Figure 5 visualizes the gradients of the water concentration on macro scale in red and on microscale x_3, in blue. Microscale x_3 is the set of PDEs on micro scale that is located furthest away from the phase boundary of the electrode (compare Figure 2). Due to its location this set of PDEs is affected last by a concentration change at the boundary of the electrode.

The plots (a), (b), and (c) of Figure 5 show the concentration gradients of the three solutions of the Two-Scale-Model from Figure 4. The water concentration on micro and macro scale is plotted over time. $C_{w,0}$ refers to the concentration on the respective scale before desorbing to $C_{w,\infty}$. For the desorption of the model anode, the sorption constant that describes the phase boundary is one, which allows the comparison of the results on the same y-axis. Therefore, the concentration on macro and micro scale are equal at the phase boundary. The colored solid lines mark the average water concentration on the scales (macro scale, red; micro scale x_0, blue). The average water concentration on macro scale (solid line) is the spatial average across the simulation domain plotted over time on the x-axis. The average water concentration on micro scale (solid line) is the spatial average across the simulation domain x_0, which is the simulation domain on micro scale located close to the mirror axis (zero-gradient boundary condition, compare Figure 2). The colored areas show the extent of the concentration gradients on each scale plotted over time on the x-axis. The concentration gradients are represented by the minimal and maximal concentration of the simulation domain (macro scale, red; micro scale x_0, blue).

Plot (a) shows the concentration gradients of the Two-Scale-Model for $\tau_{micro} \gg \tau_{macro}$. The concentration gradients on macro scale (red area) develop in the beginning and equilibrate in the first quarter of

the plotted time frame. The concentration gradients on micro scale (x_3, blue area) border the concentration gradients on macro scale because of the boundary conditions of the Two-Scale-Model. The concentration gradients on micro scale develop and remain developed over the considered time frame, confirming that the mass transport on micro scale is responsible for the extended desorption time calculated by the Two-Scale-Model for $\tau_{micro} \gg \tau_{macro}$.

Plot (b) shows the concentration gradients of the Two-Scale-Model for $\tau_{micro} \approx \tau_{macro}$. Concentration gradients on macro and micro scale develop and appear balanced over the plotted time frame. This circumstance indicates an influence of the mass transport on both scales on the overall mass transport of water in the electrode.

Plot (c) shows the concentration gradients of the Two-Scale-Model for $\tau_{micro} \ll \tau_{macro}$. The concentration gradients on macro scale develop to a larger extent compared to plot (a) and plot (b). The concentration gradients on micro scale follow the maximum concentration on macro scale without developing any concentration gradients. This indicates that the mass transport on micro scale does not affect the overall mass transport of water in the electrode. The observation agrees with the findings from Figure 4, where the Two-Scale-Model for $\tau_{micro} \ll \tau_{macro}$ returns the same solution as the pure macro scale simulation.

Applying the Two-Scale-Model to the desorption of a PVDF anode

Experimental studies show that the binder system influences the sorption of the anode significantly.[10,22] The CMC/SBR binder system absorbs more water than the PVDF binder system. Therefore, PVDF anodes absorb less water than CMC/SBR anodes while also having a different water distribution among its components. The PVDF anode used in this study consists of 5.5% PVDF and 94.5% active material (graphite) and additives (carbon black). We hypothesize that the kinetics of the desorption of the water absorbed in the PVDF is the mass-transport resistance on micro scale. Furthermore, the kinetics of the desorption of the water adsorbed to the active material and carbon black is the mass-transport resistance on macro scale. The water distribution among the macro and micro scale is simulated based on the model of weighted sums after Eser et al.[10] They showed that the weighted sums of the water content in each component of a CMC/SBR anode can approximate the water content of the anode. The model of weighted sums was applied to the PVDF anode investigated in this study based on literature sorption data.[11,22] Figure 6 shows the water distribution in the anodes at the start of the desorption in the pie chart (initial relative humidity of 50%) and the simulation of the desorption according to the Two-Scale-Model. The following results are from a simulated desorption of water from the PVDF anode that is used for the experiments in Figure 7 as well. The mass transport parameters of the PVDF anode for this simulation are given in the SI.

The y-axis plots water content in weight parts per million (wt-ppm) and x-axis time in hours. The pie-chart within this plot indicates the water distribution in the components on macro and micro scale at the beginning of the desorption. The solution of the Two-Scale-Model with $\tau_{micro} \approx \tau_{macro}$ and the solution of pure macro scale (no τ_{micro}) are shown. The color bar indicates the normalized concentration-gradient intensity micro scale. The normalized concentration gradients are calculated on the micro scale that is located furthest away from the phase boundary of the electrode (compare Figure 2) by subtracting minimal and maximal concentration for each time step and dividing this difference by the initial concentration.

11 wt% of the water absorbed in the PVDF anode can be attributed to the sorption of water in the PVDF binder. The desorption of this water may be restricted by the mass transport of water in the PVDF and as such on micro scale (compare Figure 2). The other 89% of the absorbed water can be attributed to the active material of the anode. The desorption of this water may be restricted by the gas-phase mass transport of water through the porous structure of the electrode, therefore on macro scale (compare Figure 2). Both desorption curves propagate alike. The intensity of the normalized concentration gradients on micro scale of the Two-Scale-model peaks when the deviation between the two curves is largest. This circumstance shows that the mass-transport resistance on micro scale is responsible for this deviation. As the water content in the anode approaches zero, the concentration gradients on micro scale faint.

The influence of the water mass transport on micro scale on the desorption from the anode is largest if the concentration gradients on micro scale are developed. In case of the water distribution in the PVDF anode with $\tau_{micro} \approx \tau_{macro}$, this influence is small compared to for example Figure 4. Therefore, if the diffusion times on macro and micro scale are similar for the PVDF anode, the following experiment would be predictable *via* the Two-Scale-Model and the pure macro scale simulation.

Comparing the Two-Scale-Model to experiments

A desorption experiment with a stack of PVDF anodes serves as the first verification of the Two-Scale-Model. The geometry during this desorption experiment resembles the mass transport that occurs during post-drying in either coil or stack format. The simulation of the desorption *via* the Two-Scale-Model is based on following assumptions:

- The mass-transport resistance on macro scale is the gas-phase of the porous electrode structure.
- The tortuosity of the porous structure is approximated *via* the correlation of Zehner-Bauer-Schlünder.[28]
- The water distribution among macro and micro scale is modeled according to the model of weighted sums after Eser et al.[10]
- The initial water loading of the sample was adjusted to the experimentally observed initial water loading while maintaining the aforementioned water distribution among macro and micro scale.

Porosity, mass-transport distance, and average pore size are directly measured from the sample. The diffusion coefficient of water on micro scale within the anode is unknown. Therefore, the mass-transport parameters on micro scale are adapted to best replicate the experiment. This approach finds diffusion times on macro and micro scale that describe the experiment with the Two-Scale-Model. Figure 7 shows two simulations and the results of the desorption experiment.

This figure plots water content over time. The markers show the experiment and the solid and dashed lines the simulation *via* the Two-Scale-Model. The time axis is shifted to plot negative time values. The markers before time zero show the water content of the anode stack prior to the desorption. The desorption is initiated at time zero by constantly perfusing the surrounding of the sample with dry nitrogen. This perfusion results in a decrease of water content in the sample. The water content drops below 300 wt-ppm within 15 min and transitions into a decelerated linear decrease.

The solution of the Two-Scale-Model without τ_{micro} suggests, similarly to the experiment, a fast decrease in water content in the beginning. However, the transition to the linear decrease of water content of the experiment is not predicted by this solution without τ_{micro}. Therefore, this solution predicts a faster drying than experimentally observed. The solution of the

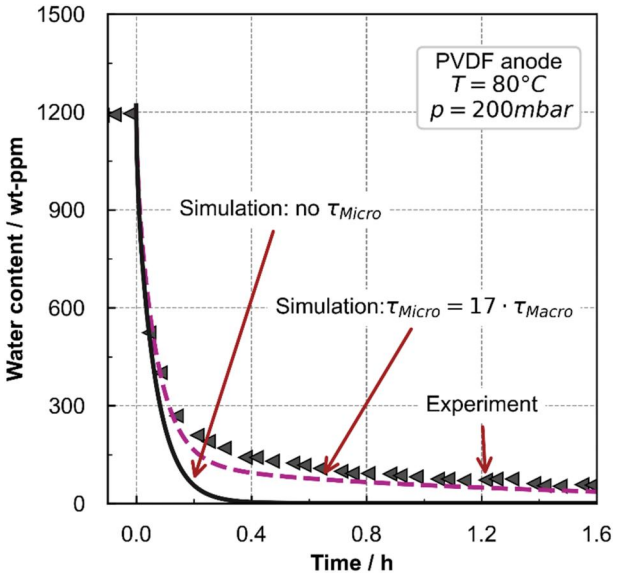

Figure 7. Comparison of an experimental desorption of stacked PVDF anodes *versus* two simulated desorption curves from the Two-Scale-Model. The simulations of the desorption were conducted with two diffusion times on micro scale. The mass transport resistance of water on macro scale is the gas phase in the porous structure of the electrodes. The solution of the Two-Scale-Model with no τ_{micro} suggests a faster desorption than experimentally observed. This solution does not show the linear desorption below 300 wt-ppm. The diffusion time of $\tau_{\mathrm{micro}} = 17 \cdot \tau_{\mathrm{macro}}$ best replicates the experimental desorption. This shows that the mass transport on macro and micro scale of the Two-Scale-Model can replicate the desorption of a PVDF anode stack.

Two-Scale-Model with $\tau_{\mathrm{micro}} = 17 \cdot \tau_{\mathrm{macro}}$ suggests a fast decrease in water content in the beginning like the experiment and the solution without τ_{micro}. The solution with $\tau_{\mathrm{micro}} = 17 \cdot \tau_{\mathrm{macro}}$ also expresses the transition toward the decelerated linear decrease like the experiment. The factor 17 was empirically chosen based on visual comparison of the various simulation results. The results show that the Two-Scale-Model with adapted diffusion times can reproduce the desorption observed in a PVDF anode stack more accurately than a model with a single constant mass-transport resistance.

However, the Two-Scale-Model with $\tau_{\mathrm{micro}} = 17 \cdot \tau_{\mathrm{macro}}$ does not perfectly replicate the experimentally observed desorption. Furthermore, $\tau_{\mathrm{micro}} = 17 \cdot \tau_{\mathrm{macro}}$ may not be physically meaningful due to the current assumptions of the Two-Scale-Model. These assumptions could be responsible for the deviation in the replication of the experiment by the Two-Scale-Model. Material properties such as the sorption equilibrium and a diffusion coefficient e.g., water in a polymer are not linear and depend on the water concentration as opposed to the assumptions of this

study. Furthermore, it is very likely that the complex microstructure of an electrode affects the mass-transport distance on micro scale. These effects can numerically be incorporated into the Two-Scale-Model, for example *via* a τ_{micro} that varies with the water concentration on micro scale. These effects and mass-transport parameters must be independently ascertained before a physically meaningful incorporation into the model is possible, which is the next step to a comprehensive validation of the Two-Scale-Model. At this point, it is unknown which mass-transport resistance is the dominant one on micro scale, which will be addressed in succeeding studies. However, the general applicability of the Two-Scale-Model was shown.

Conclusion

We propose the Two-Scale-Model for the simulation of the mass transport of water inside the composite structure of an anode, which occurs during production of LiB electrodes. The theoretical and experimental applicability of the model was shown for the water desorption from a model anode and a PVDF anode, respectively.

The diffusion times (the fraction of the effective diffusion coefficient and the mass-transport distance) were derived from the PDEs to quantify the mass-transport resistance on macro and micro scale. Solutions of the Two-Scale-Model with varying diffusion times on micro scale were compared to a one-scale simulation to verify that boundary cases are correctly replicated by the Two-Scale-Model. The concentration gradients that develop during the simulation of the desorption confirm that the Two-Scale-Model replicates boundary cases correctly. Furthermore, the concentration gradients develop according to the diffusion times, which shows consistency.

Applying the Two-Scale-Model to the water desorption of a PVDF anode showed that at equal diffusion times on macro and micro scale, the mass-transport resistance on micro scale affects the desorption very little. However, the comparison of the Two-Scale-Model to an experimental desorption shows that the Two-Scale-Model replicates the experimentally observed desorption best with $\tau_{micro} \gg \tau_{macro}$. This shows that the Two-Scale-Model can describe the desorption of water from this PVDF-anode stack, while the solution of a one-scale model cannot replicate the experimentally observed desorption. We can therefore conclude that the Two-Scale-Model is suitable to simulate mass transport in the composite structure of the LiB electrode as opposed to one-dimensional simulation approaches. A thorough validation of the Two-Scale-Model for anode and cathode with various binder systems and sample geometries should be addressed in further studies.

Acknowledgments

The authors also thank Nico Korell for simulative support and fruitful discussions.

Disclosure statement

The authors declare no conflict of interest.

Funding

This research was funded by the Federal Ministry of Research, Technology and Space (BMFTR), former Federal Ministry of Education and Research (BMBF), grant number 03XP0295A *via* the competence cluster ProZell 2.

References

[1] Kwade, A.; Haselrieder, W.; Leithoff, R.; Modlinger, A.; Dietrich, F.; Droeder, K. Current Status and Challenges for Automotive Battery Production Technologies. *Nat. Energy* **2018**, *3*, 290–300. DOI: 10.1038/s41560-018-0130-3.

[2] Huttner, F.; Haselrieder, W.; Kwade, A. The Influence of Different Post-Drying Procedures on Remaining Water Content and Physical and Electrochemical Properties of Lithium-Ion Batteries. *Energy Technol.* **2020**, *8*, 1900245. DOI: 10.1002/ente.201900245.

[3] Saharan, V.; Roberts, J.; Manev, V.; Chia, Y. H.; MacLean, G.; McMullen, S. R. Moisture-Uptake by the Positive Active Material from the Casting Solvent and the Ambient Environment. *J. Power Sources* **2005**, *146*, 809–812. DOI: 10.1016/j.jpowsour.2005.03.088.

[4] Bryntesen, S. N.; Strømman, A. H.; Tolstorebrov, I.; Shearing, P. R.; Lamb, J. J.; Stokke Burheim, O. Opportunities for the State-of-the-Art Production of LIB Electrodes—A Review. *Energies (Basel)* **2021**, *14*, 1406. DOI: 10.3390/en14051406.

[5] Kaiser, J.; Wenzel, V.; Nirschl, H.; Bitsch, B.; Willenbacher, N.; Baunach, M.; Schmitt, M.; Jaiser, S.; Scharfer, P.; Schabel, W. Prozess- Und Produktentwicklung Von Elektroden Für Li-Ionen-Zellen. *Chem. Ing. Technol.* **2014**, *86*, 695–706. DOI: 10.1002/cite.201300085.

[6] Huttner, F.; Marth, A.; Eser, J. C.; Heckmann, T.; Mohacsi, J.; Mayer, J. K.; Scharfer, P.; Schabel, W.; Kwade, A. Design of Vacuum Post-Drying Procedures for Electrodes of Lithium-Ion Batteries. *Batteries Supercaps* **2021**, *4*, 1499–1515. DOI: 10.1002/batt.202100088.

[7] Degen, F.; Winter, M.; Bendig, D.; Tübke, J. Energy Consumption of Current and Future Production of

Lithium-Ion and Post Lithium-Ion Battery Cells. *Nat. Energy* **2023**, *8*, 1284–1295. DOI: 10.1038/s41560-023-01355-z.

[8] Schünemann, J.-H.; Dreger, H.; Bockholt, H.; Kwade, A. Smart Electrode Processing for Battery Cost Reduction. *ECS Trans.* **2016**, *73*, 153–159. DOI: 10.1149/07301.0153ecst.

[9] Thomitzek, M.; Schmidt, O.; Röder, F.; Krewer, U.; Herrmann, C.; Thiede, S. Simulating Process-Product Interdependencies in Battery Production Systems. *Proc. CIRP* **2018**, *72*, 346–351. DOI: 10.1016/j.procir.2018.03.056.

[10] Eser, J. C.; Wirsching, T.; Weidler, P. G.; Altvater, A.; Börnhorst, T.; Kumberg, J.; Schöne, G.; Müller, M.; Scharfer, P.; Schabel, W. Moisture Adsorption Behavior in Anodes for Li-Ion Batteries. *Energy Technol.* **2020**, *8*, 1801162. DOI: 10.1002/ente.201801162.

[11] Eser, J. C.; Deichmann, B.; Wirsching, T.; Weidler, P. G.; Scharfer, P.; Schabel, W. Hysteresis Behavior in the Sorption Equilibrium of Water in Anodes for Li-Ion Batteries. *Langmuir* **2020**, *36*, 6193–6201. DOI: 10.1021/acs.langmuir.0c00704.

[12] Eser, J. C.; Deichmann, B.; Wirsching, T.; Merklein, L.; Müller, M.; Scharfer, P.; Schabel, W. Diffusion Kinetics of Water in Graphite Anodes for Li-Ion Batteries. *Dry. Technol.* **2022**, *40*, 1130–1145. DOI: 10.1080/07373937.2020.1852568.

[13] Huttner, F.; Diener, A.; Heckmann, T.; Eser, J. C.; Abali, T.; Mayer, J. K.; Scharfer, P.; Schabel, W.; Kwade, A. Increased Moisture Uptake of NCM622 Cathodes after Calendering Due to Particle Breakage. *J. Electrochem. Soc.* **2021**, *168*, 090539. DOI: 10.1149/1945-7111/ac24bb.

[14] Heckmann, T.; Eser, J. C.; Altvater, A.; Dörr, J.; Lepère, H.; Scharfer, P.; Schabel, W. Mass Transport in the Stefan-Knudsen Transition Region during Vacuum Drying at Different Pressures in a Porous Structure Resembling Battery Electrodes. *Langmuir* **2023**, *39*, 2859–2869. DOI: 10.1021/acs.langmuir.2c03450.

[15] Schuer, A. R.; Kuenzel, M.; Yang, S.; Kosfeld, M.; Mueller, F.; Passerini, S.; Bresser, D. Diagnosis Tools for Humidity-Born Surface Contaminants on Li[Ni0.8Mn0.1Co0.1]O2 Cathode Materials for Lithium Batteries. *J. Power Sources* **2022**, *525*, 231111. DOI: 10.1016/j.jpowsour.2022.231111.

[16] Kosfeld, M.; Westphal, B.; Kwade, A. Moisture Behavior of Lithium-Ion Battery Components along the Production Process. *J. Energy Storage* **2023**, *57*, 106174. DOI: 10.1016/j.est.2022.106174.

[17] Zou, L.; He, Y.; Liu, Z.; Jia, H.; Zhu, J.; Zheng, J.; Wang, G.; Li, X.; Xiao, J.; Liu, J.; et al. Unlocking the Passivation Nature of the Cathode–Air Interfacial Reactions in Lithium Ion Batteries. *Nat. Commun.* **2020**, *11*, 3204. DOI: 10.1038/s41467-020-17050-6.

[18] Sicklinger, J.; Metzger, M.; Beyer, H.; Pritzl, D.; Gasteiger, H. A. Ambient Storage Derived Surface Contamination of NCM811 and NCM111: Performance Implications and Mitigation Strategies. *J. Electrochem. Soc.* **2019**, *166*, A2322–A2335. DOI: 10.1149/2.0011912jes.

[19] Jung, R.; Morasch, R.; Karayaylali, P.; Phillips, K.; Maglia, F.; Stinner, C.; Shao-Horn, Y.; Gasteiger, H. A. Effect of Ambient Storage on the Degradation of Ni-Rich Positive Electrode Materials (NMC811) for Li-Ion Batteries. *J. Electrochem. Soc.* **2018**, *165*, A132–A141. DOI: 10.1149/2.0401802jes.

[20] Heckmann, T.; Madlindl, L.; Scharfer, P.; Schabel, W. Increased Water Uptake of Li[Ni $_{0.6}$ Co $_{0.2}$ Mn $_{0.2}$] O $_{2}$ for Lithium-Ion Batteries in Humid Nitrogen above a Critical Gas Dew Point. *ACS Appl. Energy Mater.* **2024**, *7*, 1882–1889. DOI: 10.1021/acsaem.3c02976.

[21] Stich, M.; Pandey, N.; Bund, A. Drying and Moisture Resorption Behaviour of Various Electrode Materials and Separators for Lithium-Ion Batteries. *J. Power Sources* **2017**, *364*, 84–91. DOI: 10.1016/j.jpowsour.2017.08.009.

[22] Heckmann, T.; Eser, J. C.; Altvater, A.; Streller, N.; Scharfer, P.; Schabel, W. Experimental Investigation of the Temperature, Pressure, and Binder System Influence on Vacuum Postdrying Processes and Moisture Management of Li-Ion Battery Electrodes. *Energy Technol.* **2023**, *11*, 2200859. DOI: 10.1002/ente.202200859.

[23] Jaiser, S.; Kumberg, J.; Klaver, J.; Urai, J. L.; Schabel, W.; Schmatz, J.; Scharfer, P. Microstructure Formation of Lithium-Ion Battery Electrodes during Drying – an Ex-Situ Study Using Cryogenic Broad Ion Beam Slope-Cutting and Scanning Electron Microscopy (Cryo-BIB-SEM). *J. Power Sources* **2017**, *345*, 97–107. DOI: 10.1016/j.jpowsour.2017.01.117.

[24] Schiesser, W. E.; Griffiths, G. W. *A Compendium of Partial Differential Equation Models;* Cambridge University Press: Cambridge, **2009**. https://www.cambridge.org/us/universitypress/subjects/mathematics/numerical-analysis/compendium-partial-differential-equation-models-method-lines-analysis-matlab?format=HB&isbn=9780521519861.

[25] Schabel, W.; Scharfer, P.; Kind, M.; Mamaliga, I. Sorption and Diffusion Measurements in ternary polymer–Solvent–Solvent Systems by Means of a Magnetic Suspension Balance—Experimental Methods and Correlations with a Modified Flory–Huggins and Free-Volume Theory. *Chem. Eng. Sci.* **2007**, *62*, 2254–2266. DOI: 10.1016/j.ces.2006.12.062.

[26] J. Kärger D. M.; Ruthven *Theodōru, Diffusion in Nanoporous Materials*; Wiley-VCH-Verl: Weinheim, **2012**.

[27] Eser, J. Über das Stofftransport- und Sorptionsverhalten im Nachtrocknungsprozess von Elektroden für Li-Ionen-Batterien, **2021**.

[28] Zehner, P.; Schlünder, E. U. Wärmeleitfähigkeit Von Schüttungen Bei Mäßigen Temperaturen. *Chem. Ing. Technol.* **1970**, *42*, 933–941. DOI: 10.1002/cite.330421408.